



CRYO-ELECTRON MICROSCOPY DATA DENOISING BASED ON THE GENERALIZED DIGITIZED TOTAL VARIATION METHOD

QIN ZHANG* and CHANDRAJIT L. BAJAJ**

Institute for Computational Engineering and Sciences
University of Texas
Austin, TX 78712, U. S. A.
e-mail: zqyork@ices.utexas.edu

CVC, Department of Computer Science
Institute for Computational Engineering and Sciences
University of Texas
Austin, TX 78712, U. S. A.
e-mail: bajaj@cs.utexas.edu

Abstract

The energy functional used in digitalized total variation method is expanded to a general form and a generalized digitized total variation (GDTV) denoising method is obtained. We further expand this method from 2-dimensional (2D) image to 3-dimensional (3D) image processing field. Cryo-electron microscopy (cryo EM) and single particle reconstruction are becoming part of standard collection of structural techniques used for studying macromolecular assemblies. However, the 3D data obtained suffers greatly from noise and degradation for the low

2000 Mathematics Subject Classification: **Kindly Provide.**

Keywords and phrases: Cryo-electron microscopy (cryoEM), image denoising, generalized digitized total variation (GDTV), variational method.

*Supported in part by NIH contracts R01-GM074258, R01-GM07308, R01-EB004873.

**Supported in part by NSF Grant CNS-0540033 and NIH contracts P20-RR020647, R01-GM074258, R01-GM07308, R01-EB004873.

Received October 27, 2009

dose electron radiation. Thus, image enhancement and noise reduction are theoretically necessary to improve the data for the subsequent segmentation and/or structure skeletonization. Although there are several methods to tackle this problem, we are pleased to find that GDTV method is very efficient and can achieve better performance. Comparative experiments are carried out to verify the enhancement achieved by the GDTV method.

1. Introduction

As an emerging technology, Cryo-electron microscopy (cryoEM) has shown to be powerful in solving the 3D structure of large macromolecular assemblies and cellular complexes [3, 14], which are always beyond the capability of x-ray crystallography and NMR spectroscopy techniques by today. Since some of the biological molecules are sensitive to high energy electron radiations, imaging must be conducted using low dose conditions [15] to keep the sampling species in an in vivo status. Therefore, the images obtained by cryoEM technique are extremely noisy compared to other imaging techniques. Before putting the volume data into Electron Microscopy Data Bank (EMDB) (<http://www.ebi.ac.uk/msd/emdb/>), the modeling and computational errors of different techniques of transferring 2D image data into volume data also contribute extra levels of noise. Therefore, noise reduction and image enhancement are desirable for 3D reconstruction, segmentation and/or structural analysis, such as skeletonization.

A large number of image filters have been developed to decrease the noise, such as [16] low pass filter, wavelet transforms, median filters, and so on. What makes denoising so challenging is that a successful approach must also preserve characteristic singular features of images such as edges. In the past decades, deterministic and stochastic models were proposed to solve this problem. In many monographs, such as [1, 9], image denoising is almost the most important topic. In [18], bilateral filter is applied to denoise the cryoEM data. During our experiments, bilateral filtering sometimes oversmooths the cryoEM data and is very time consuming. As two tightly linked methods, variational methods and Partial Differential Equation (PDE) methods have been successful tools in image processing in recent years. For a given image, one can define an energy functional which characterizes the smoothness and the features in continuous setting, then compute the variation for the functional to gain an Euler-Lagrange equation. Thus, a steady

state equation or an evolution equation can be solved to get the minimizer which is regarded as the improved version of the image. On the other hand, many PDEs used in image processing can be deduced from energy functionals. We assume that $u : \Omega \subset \mathbb{R}^3 \rightarrow \mathbb{R}$ is an original image, and u^0 is the observed image, which is always treated as a degraded version of u . The process is usually modeled as $u^0 = Ru + n$ with n as noise part and R a blurring operator. In this paper, R is selected as I operator since we focus merely on denoising problem other than deblurring problem. According to the well-posedness theory of Hadamard, image denoising problem, as an inverse problem, is always ill-posed. Based on the theory of Tikhonov regularization, a widely adapted technique to circumvent this ill-posedness difficulty, is to minimize the following regularized minimization problem,

$$E(u) = \int_{\Omega} \phi(\|\nabla u\|) dx + \frac{\lambda}{2} \int_{\Omega} (u - u^0)^2 dx, \quad (1)$$

where the first term is used as a regular term to represent the smoothness of the image and the second term measures the fidelity to the original data. And positive parameter λ weighs these two parts and is always user-defined. Function ϕ is selected to depict the strength of the smoothness and is usually chosen as $\phi(x) = x^2$ (the corresponding energy of the first term is Dirichlet energy) and $\phi(x) = x$ (the corresponding energy of the first term is usually named as total variation), which are actually L^2 and L^1 norm of functions.

The differential equations (either the steady status equation or the evolution equation) from the energy functional (1) are discretized numerically on a rectangular grid. A large number of publications have appeared (see, for example, [21, 26, 27]) in the past decades. Since the Euler-Lagrange equation associated with (1) is usually a nonlinear PDE, when applying it to a digital image, one has to carefully choose numerical schemes to take care of the nonlinearity. Later, Osher and Shen [23] established a self-contained “digital” theory for the PDE method, in which knowledge of PDEs and numerical approximations is not required. The “digital” method does not mean the discrete numerical implementation of the existing differential equations. Instead, the method starts directly with the discrete variational problem, from which algebraic equilibrium equations analogous to the PDEs are established. It is unnecessary to search for the meaning of these algebraic equations

from their PDE counterparts. Remarkably, the underlying domain can fairly be irregular. Motivated by the theory of [23], in [28, 31], we proposed to digitalize the energy (1) to obtain a general formulation for image denoising. An ideal graph model is considered and regularization operation for the local variation is avoided. This formulation is implemented by a local iterative scheme which is more efficient than usual PDE methods since there is no necessity to solve a linear system. The method is named as generalized digitized total variation method (GDTV for short abbreviation). In [4, 5], Bougleux et al. proposed one discrete regularization framework on weighted graphs of arbitrary topology for image and mesh filtering, where the regularization term comes from a special integral in (1).

In this paper, we expand the proposed GDTV method to 3D cryoEM data. Numerical experiments are carried out and comparative examples are presented to show the performance of GDTV method. We also integrated into our in-house software VolRover <http://cvcweb.ices.utexas.edu/software/#VolRover> for volume image processing.

The remainder of the paper is organized as follows. In Section 2, the graph model, energy functional and denoising equation are expanded to 3D case. The algorithm is sketched in Section 3. Large number of numerical experiments and comparative examples are presented in Section 4. Section 5 concludes the paper.

2. Graph Model, Energy Functional and Denoising Equation

2.1. Basic definitions for a graph

For a 3D digital image $u : \Omega \rightarrow \mathbb{R}$, let $[\Omega, G]$ denote an undirected graph with a finite set Ω of voxels (or nodes) and a dictionary G of edges. The graph is assumed to have no self-loops and general vertices are denoted by α, β, \dots (cf. Figure 1). If α and β are linked by an edge with length r , then we write $\alpha \stackrel{r}{\sim} \beta$. We use

$$N_1 = \{\beta \in \Omega; \beta \stackrel{1}{\sim} \alpha\},$$

$$N_{\sqrt{2}} = \{\gamma \in \Omega; \gamma \stackrel{\sqrt{2}}{\sim} \alpha\},$$

$$N_{\sqrt{3}} = \{\delta \in \Omega; \delta \stackrel{\sqrt{3}}{\sim} \alpha\}$$

to denote the 1, $\sqrt{2}$ and $\sqrt{3}$ -neighbors of α , respectively. For each voxel α in a 3D

image, there are always six 1-neighbors, twelve $\sqrt{2}$ -neighbors, and eight $\sqrt{3}$ -neighbors. The value at vertex α is denoted by u_α . Similar to the definition of length of gradient ∇u , we define the *local variation* or *strength* $\|\nabla_g u_\alpha\|$ of its digital version at any voxel α as

$$\|\nabla_g u_\alpha\| := \sqrt{\sum_{\beta \sim \alpha} (u_\beta - u_\alpha)^2 + \sum_{\gamma \sim \alpha} \frac{(u_\gamma - u_\alpha)^2}{2} + \sum_{\delta \sim \alpha} \frac{(u_\delta - u_\alpha)^2}{3}}.$$

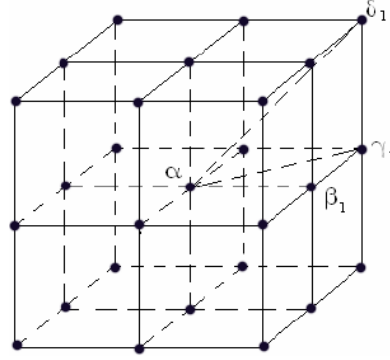


Figure 1. Vertex α and its neighborhood.

Expanding the notations in [8], we define the *edge derivative*. Let e, f and h be the edges $\alpha \sim \beta$, $\alpha \sim \gamma$ and $\alpha \sim \delta$, respectively. Then the edge derivatives of u along e, f and h are correspondingly defined to be

$$\left. \frac{\partial u}{\partial e} \right|_\alpha := u_\beta - u_\alpha, \quad \left. \frac{\partial u}{\partial f} \right|_\alpha := \frac{u_\gamma - u_\alpha}{\sqrt{2}} \quad \text{and} \quad \left. \frac{\partial u}{\partial h} \right|_\alpha := \frac{u_\delta - u_\alpha}{\sqrt{3}}.$$

We can also write

$$\|\nabla_g u_\alpha\| = \sqrt{\sum_{e \vdash \alpha} \left[\left. \frac{\partial u}{\partial e} \right|_\alpha \right]^2 + \sum_{f \vdash \alpha} \left[\left. \frac{\partial u}{\partial f} \right|_\alpha \right]^2 + \sum_{h \vdash \alpha} \left[\left. \frac{\partial u}{\partial h} \right|_\alpha \right]^2},$$

where $e \vdash \alpha$, $f \vdash \alpha$ and $h \vdash \alpha$ represent that α is a 1-node of e , a $\sqrt{2}$ -node of f and a $\sqrt{3}$ -node of h .

2.2. Digitalized energy and equations

Similar to [31], the fitted digitalized version for energy functional (1) is

$$\mathcal{E}(u) := \sum_{\alpha \in \Omega} \phi(\|\nabla_g u_\alpha\|) + \frac{\lambda}{2} \sum_{\alpha \in \Omega} (u_\alpha - u_\alpha^0)^2, \quad (2)$$

where function $\phi(x)$ is simply chosen as Kim and Lim in [19] as $\phi(x) = x^{2-q}$, $0 \leq q < 2$. Obviously, $\phi(x)$ can be selected as other forms, such as listed in [1, p. 83]

$$\phi(x) = \frac{x^2}{1+x^2}, \log(1+x^2), 2\sqrt{1+x^2} - 2, \text{ etc.}$$

Theorem 1. *With respect to digitalized energy (2), the denoising equation is*

$$\begin{aligned} 0 &= \sum_{\beta \in N_1} (u_\alpha - u_\beta) \left(\frac{\phi'(\|\nabla_g u_\alpha\|)}{\|\nabla_g u_\alpha\|} + \frac{\phi'(\|\nabla_g u_\beta\|)}{\|\nabla_g u_\beta\|} \right) \\ &+ \sum_{\gamma \in N_{\sqrt{2}}} \frac{u_\alpha - u_\gamma}{2} \left(\frac{\phi'(\|\nabla_g u_\alpha\|)}{\|\nabla_g u_\alpha\|} + \frac{\phi'(\|\nabla_g u_\gamma\|)}{\|\nabla_g u_\gamma\|} \right) \\ &+ \sum_{\delta \in N_{\sqrt{3}}} \frac{u_\alpha - u_\delta}{3} \left(\frac{\phi'(\|\nabla_g u_\alpha\|)}{\|\nabla_g u_\alpha\|} + \frac{\phi'(\|\nabla_g u_\delta\|)}{\|\nabla_g u_\delta\|} \right) + \lambda(u_\alpha - u_\alpha^0), \quad \alpha \in \Omega. \quad (3) \end{aligned}$$

We omit the proof of this theorem, the interested reader can write it out according to the idea of [31].

Corollary 1. *If $\phi(x) = x^{2-q}$, $0 \leq q < 2$, then (3) turns out to be*

$$\begin{aligned} 0 &= (2-q) \left(\sum_{\beta \in N_1} (u_\alpha - u_\beta) (\|\nabla_g u_\alpha\|^{-q} + \|\nabla_g u_\beta\|^{-q}) \right. \\ &+ \sum_{\gamma \in N_{\sqrt{2}}} \frac{u_\alpha - u_\gamma}{2} (\|\nabla_g u_\alpha\|^{-q} + \|\nabla_g u_\gamma\|^{-q}) \\ &\left. + \sum_{\delta \in N_{\sqrt{3}}} \frac{u_\alpha - u_\delta}{3} (\|\nabla_g u_\alpha\|^{-q} + \|\nabla_g u_\delta\|^{-q}) \right) + \lambda(u_\alpha - u_\alpha^0), \quad \alpha \in \Omega. \quad (4) \end{aligned}$$

In the following experiments, we only select $\phi(x) = x^{2-q}$, $0 \leq q < 2$.

Corollary 2. Equation (3) is the digital version of

$$\operatorname{div}\left(\phi'(\|\nabla u\|)\frac{\nabla u}{\|\nabla u\|}\right) + \lambda(u^0 - u) = 0, \quad (5)$$

which is the Euler-Lagrange equation of (1).

We also omit the proof for the similarity to the proof in [31].

3. Detailed Denoising Algorithm

For a voxel α being dealt with, if $\|\nabla_g u_\alpha\| \neq 0$, $\|\nabla_g u_\beta\| \neq 0$, $\|\nabla_g u_\gamma\| \neq 0$ and $\|\nabla_g u_\delta\| \neq 0$, we define weight functions

$$\omega_{\alpha\beta}(u) = \frac{\phi'(\|\nabla_g u_\alpha\|)}{\|\nabla_g u_\alpha\|} + \frac{\phi'(\|\nabla_g u_\beta\|)}{\|\nabla_g u_\beta\|}, \quad (6)$$

$$\omega_{\alpha\gamma}(u) = \frac{\phi'(\|\nabla_g u_\alpha\|)}{2\|\nabla_g u_\alpha\|} + \frac{\phi'(\|\nabla_g u_\gamma\|)}{2\|\nabla_g u_\gamma\|}, \quad (7)$$

$$\omega_{\alpha\delta}(u) = \frac{\phi'(\|\nabla_g u_\alpha\|)}{3\|\nabla_g u_\alpha\|} + \frac{\phi'(\|\nabla_g u_\delta\|)}{3\|\nabla_g u_\delta\|}. \quad (8)$$

If $\|\nabla_g u_\alpha\| = 0$, then we define $\omega_{\alpha\beta}(u) = \omega_{\alpha\gamma}(u) = \omega_{\alpha\delta}(u) = 0$. If $\|\nabla_g u_\alpha\| \neq 0$ and $\|\nabla_g u_\beta\|$, $\|\nabla_g u_\gamma\|$, or $\|\nabla_g u_\delta\|$ vanishes, we first prescribe $\|\nabla_g u_\beta\|$, $\|\nabla_g u_\gamma\|$, or $\|\nabla_g u_\delta\|$ is a small positive number a (e.g., 10^{-4}), and then define weight function according to (6), (7) and (8).

Then equation (3) becomes

$$\begin{aligned} & \left(\lambda + \sum_{\beta \in N_1} \omega_{\alpha\beta}(u) + \sum_{\gamma \in N_{\sqrt{2}}} \omega_{\alpha\gamma}(u) + \sum_{\delta \in N_{\sqrt{3}}} \omega_{\alpha\delta}(u) \right) u_\alpha \\ & - \sum_{\beta \in N_1} \omega_{\alpha\beta}(u) u_\beta - \sum_{\gamma \in N_{\sqrt{2}}} \omega_{\alpha\gamma}(u) u_\gamma - \sum_{\delta \in N_{\sqrt{3}}} \omega_{\alpha\delta}(u) u_\delta = \lambda u_\alpha^0, \end{aligned} \quad (9)$$

for all $\alpha \in \Omega$. This is usually a system of nonlinear equations. For simplicity, we further define

$$h_{\alpha\beta}(u) = \frac{\omega_{\alpha\beta}(u)}{\lambda + \sum_{\beta \in N_1} \omega_{\alpha\beta}(u) + \sum_{\gamma \in N_{\sqrt{2}}} \omega_{\alpha\gamma}(u) + \sum_{\delta \in N_{\sqrt{3}}} \omega_{\alpha\delta}(u)}, \quad (10a)$$

$$h_{\alpha\gamma}(u) = \frac{\omega_{\alpha\gamma}(u)}{\lambda + \sum_{\beta \in N_1} \omega_{\alpha\beta}(u) + \sum_{\gamma \in N_{\sqrt{2}}} \omega_{\alpha\gamma}(u) + \sum_{\delta \in N_{\sqrt{3}}} \omega_{\alpha\delta}(u)}, \quad (10b)$$

$$h_{\alpha\delta}(u) = \frac{\omega_{\alpha\delta}(u)}{\lambda + \sum_{\beta \in N_1} \omega_{\alpha\beta}(u) + \sum_{\gamma \in N_{\sqrt{2}}} \omega_{\alpha\gamma}(u) + \sum_{\delta \in N_{\sqrt{3}}} \omega_{\alpha\delta}(u)}, \quad (10c)$$

$$h_{\alpha\alpha}(u) = \frac{\lambda}{\lambda + \sum_{\beta \in N_1} \omega_{\alpha\beta}(u) + \sum_{\gamma \in N_{\sqrt{2}}} \omega_{\alpha\gamma}(u) + \sum_{\delta \in N_{\sqrt{3}}} \omega_{\alpha\delta}(u)}. \quad (10d)$$

One can easily check that $h_{\alpha\alpha} + h_{\alpha\beta} + h_{\alpha\gamma} + h_{\alpha\delta} = 1$.

To solve the system of equations (9), the simplest local iteration is the Gauss-Jacobi method

$$\begin{aligned} u_\alpha^{k+1} &= \sum_{\beta \in N_1} h_{\alpha\beta}(u^k) u_\beta^k + \sum_{\gamma \in N_{\sqrt{2}}} h_{\alpha\gamma}(u^k) u_\gamma^k \\ &\quad + \sum_{\delta \in N_{\sqrt{3}}} h_{\alpha\delta}(u^k) u_\delta^k + h_{\alpha\alpha}(u^k) u_\alpha^0 \end{aligned} \quad (11)$$

for all $\alpha \in \Omega$, where k denotes the iteration step. This process can be independently explained as a forced local low-pass digital filter. The update u_α is a weighted average of the existing u_β on its 1-neighborhood and u_γ on its $\sqrt{2}$ -neighborhood and u_δ on its $\sqrt{3}$ -neighborhood and the raw data at α . The raw data serves as an attracting force preventing u from wandering too far.

Another possible scheme for (9) is Gauss-Seidel method. We omit this here for saving space. The interested reader can write it out according to the schemes in [23].

From the iterative scheme (11), the algorithm can be given as follows.

Filtering algorithm

- (1) Assign a linear order to all voxels: $\alpha_1 < \alpha_2 < \dots < \alpha_{|\Omega|}$. Set $k = 0$.
- (2) $k = k + 1$. For each voxel α , calculate local variation $\|\nabla_g u_\alpha\|$.
- (3) For each voxel α and all its 1-neighbors β , $\sqrt{2}$ -neighbors γ and $\sqrt{3}$ -neighbors δ , calculate the weighted functions $\omega_{\alpha\beta}(u^k)$, $\omega_{\alpha\gamma}(u^k)$ and $\omega_{\alpha\delta}(u^k)$ according to (6), (7) and (8), respectively.
- (4) For each voxel α , compute $h_{\alpha\beta}(u)$, $h_{\alpha\gamma}(u)$, $h_{\alpha\delta}(u)$, $h_{\alpha\alpha}(u)$ according to (10).
- (5) For each voxel α , compute u_α^{k+1} according to (11).
- (6) If $k > N$ (a prescribed iteration step) or other termination condition is satisfied, stop. Otherwise, go to (2).

4. Numerical Experiments and Comparative Results

Numerical experiments and comparative results are presented in this section. All the experiments are carried out on a Sun computer with Ubuntu 8.04 operating system. Before we present numerical experiments and comparative results, some preliminary introduction of 3D cryoEM and our test sample GroEL is provided.

Three-dimensional EM imaging plays a unique role in structural biology for its capability of revealing the three dimensional structures of biological units. The major difficulty with EM images is due to the extremely low signal-to-noise ratio (SNR). This is true partially because the electron dose used in EM imaging has to be kept in a very low level (approximately $0.5 \sim 4 e/\text{\AA}^2$) in order to reduce the radiation damage of electrons in the specimen. The flash cooling technique, known as Cryo-EM, is to quickly cool the samples to liquid nitrogen temperature (about 77K or less) such that the surrounding water does not form crystalline ice. This technique proved to be very successful in preserving the native structures of specimen while reducing the radiation damages [11].

GroE is the prototypical type I chaperonin, required for proper folding of a wide range of substrate proteins [12, 22]. It acts as an Anfinsen cage [13] to facilitate substrate folding by providing an appropriate chemical environment and can induce partial substrate unfolding during encapsulation [17]. GroE consists of two proteins, GroEL and GroES, with 14 monomers of GroEL forming two back-to-back, seven-membered rings [7]. The structure of GroEL has been studied by X-ray crystallography and Cryo-EM, resulting in nearly two dozen structural models in a variety of chemical conditions and functional states [6, 10, 25, 29]. These structural studies have provided “snapshots” of the GroE in different conformations, from which mechanistic models have been proposed. In the following experiments, all original data comes from EMDB. For 4.2Å GroEL data EMDB ID is 5001 and 6Å GroEL data EMDB ID is 1081.

Since the focus of this paper is to denoise 3D EM data, we will not mention the important topics, such as the effects of the convex and concave properties of function ϕ , pepper and salt noise removal, color image denoising by GDTV and time consuming of GDTV vs PDE methods. The interested reader is referred to [31] for details. We take only GroEL for testing the GDTV method and do comparisons.

4.1. Comparison between denoising with GDTV vs non-denoising

In this subsection, we compare the segmentation results of 3D GroEL data at 4.2Å resolution with GDTV denoising and without denoising. In [20], Ludtke et al. presented the structure reconstruction of GroEL with D7 symmetry. In Figure 2, we show the initial GroEL EM data in (a), (b) show the result of Ludtke et al. published in [20]. In Figure (c), our result is shown. We obtain the result according to the following several steps. (1) We use digitized total variation (DTV, that is $q = 1.0$ in 4) method to denoise the initial volumetric data of (a), the parameters $q = 1.0$, $\lambda = 0.0001$ in (4), iteration step is 1. We use 1-neighborhood for simplicity. (2) Using the segmentation method of [2], we segment the en bloc data into 14 subunits. (3) Use GDTV to denoise each subunit. Here we use parameters $q = 0.8$, $\lambda = 0.0001$, iteration step is 3 and use 1-neighborhood for simplicity. From these figures, we can see that our result is smoother and more features can be discerned, especially in the top and the bottom parts.

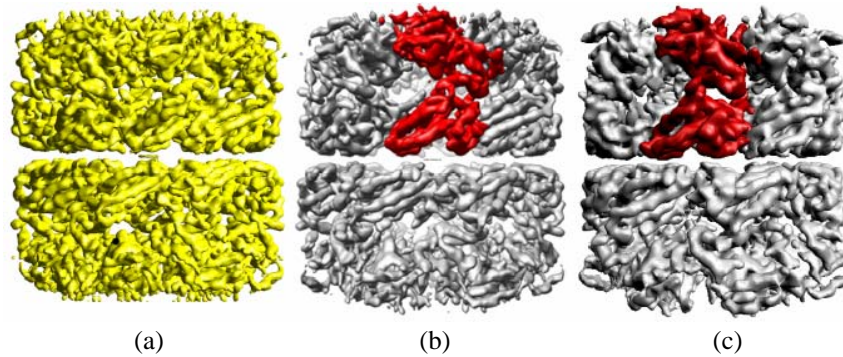


Figure 2. Comparative results between GDTV denoising and non-denoising. (a) shows the original density map. (b) shows the structure reconstruction result in Figure 1.B of [20]. (c) shows our structure reconstruction.

For 6Å GroEL density map, we show a similar example. In Figure 3(a), the original density map is shown. (b) shows the result of structure reconstruction after segmentation [2]. (c) shows the result of structure reconstruction after denoising each segmented subunit with GDTV. Our result is obviously better than the result shown in (b).

4.2. Comparison between DTV with GDTV

The difference between DTV with our GDTV method is compared in this subsection. We carry out this experiment as follows. First use DTV to denoise the original volume density map. Then use the segmentation methods as above to obtain 14 subunits. Next for each subunit, we use different parameters to do comparisons. In Figure 4, (a) shows the result after denoising the original density map (2 (a)) with GDTV method, parameters are the same as the above example. (b) shows the result after denoising each subunit by DTV method. The parameters $q = 1.0$, $\lambda = 0.0001$, iteration step is 1. We use 1-neighborhood for simplicity. (c) shows the result after denoising each subunit by GDTV method. We use parameters $q = 0.8$, 0.0001 , iteration step is 3 and use 1-neighborhood for simplicity. In Figure 5, we show one subunit for comparison, where (a), (b) and (c) show one subunit of (a), (b) and (c) of Figure 4, separately. From these figures, we can see that the difference is not very big. But we think more iteration will yield big difference.

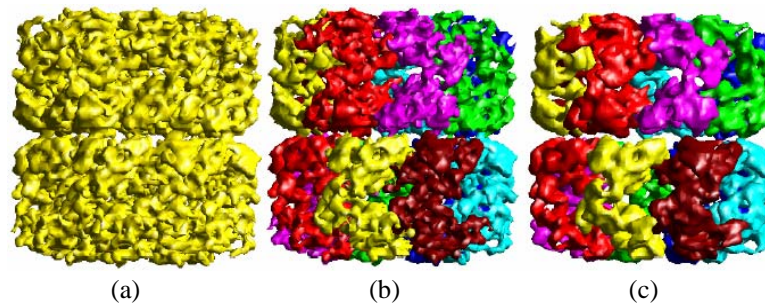


Figure 3. Comparative results between GDTV denoising and non-denoising. (a) shows the original density map of GroEL at 6Å resolution. (b) shows the result without denoising. (c) shows the structure reconstruction result after denoising each subunit with GDTV.

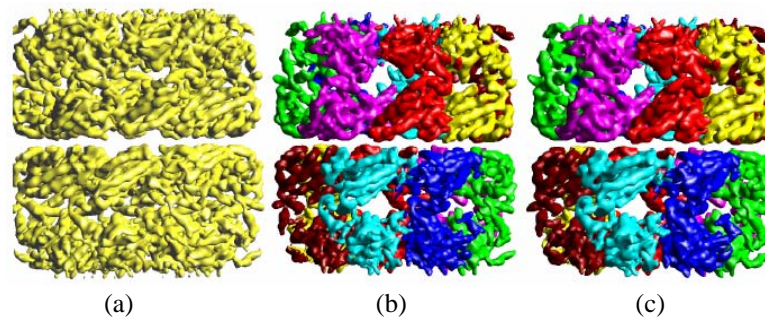


Figure 4. Comparative results between DTV and GDTV. (a) shows result after denoising the original density map with DTV. (b) shows the structure reconstruction result after denoising each subunit with DTV. (c) shows the structure reconstruction result after denoising each subunit with GDTV.

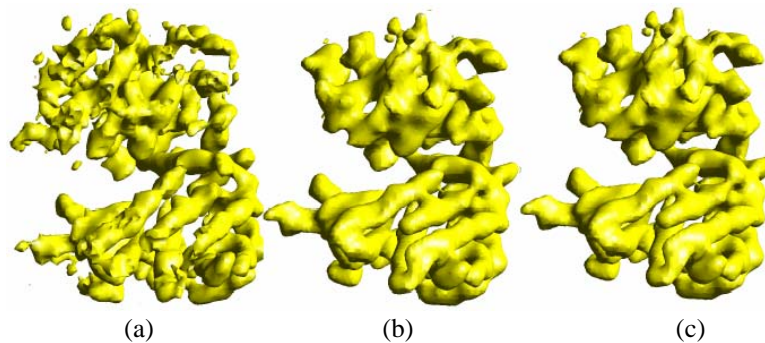


Figure 5. Comparative results between DTV and GDTV. (a), (b) and (c) show one subunit of (a), (b) and (c) of Figure 4.

4.3. Comparison between bilateral filtering and GDTV

In [18], Jiang et al. used bilateral filtering to denoise 3D EM data. During our using their code to do smoothing, we find that in some cases bilateral filtering oversmooths the density map that the obtained result is not desirable. In this subsection, we compare the results of GDTV method with bilateral filtering. The experiment is carried out as follows. In Figure 6(a) we show the initial data. In Figure (b), we show the result of bilateral filtering with default parameters. For more details on the parameters, the interested reader is referred to [18]. In Figure (c), we show the result of GDTV with default parameters. In Figure 7, one subunit of (a), (b) and (c) of Figure 6 is shown, respectively.

In Figure 8, we show another example on the difference of bilateral filtering and GDTV. For 6Å GroEL data, we use one subunit of the result of [2, 30] as test. One subunit of segmentation result is shown in Figure (a). It is obvious that the noise is heavy. In Figure (b), we show the result of bilateral filtering. We can find that oversmoothing phenomenon occurs. The result is too smooth to discern features. Our result by GDTV is shown in Figure (c). We can discern features of the subunit while smooth it.

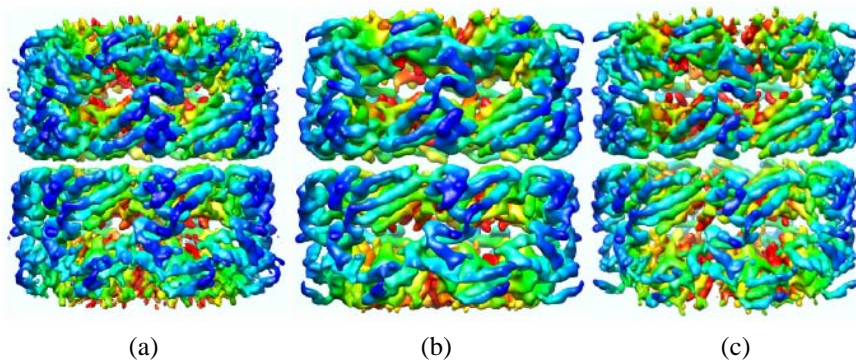


Figure 6. Comparative results between bilateral filtering and GDTV. (a) shows the original density map. (b) shows the structure reconstruction result after denoising each subunit with bilateral filtering. (c) shows the structure reconstruction result after denoising each subunit with GDTV.

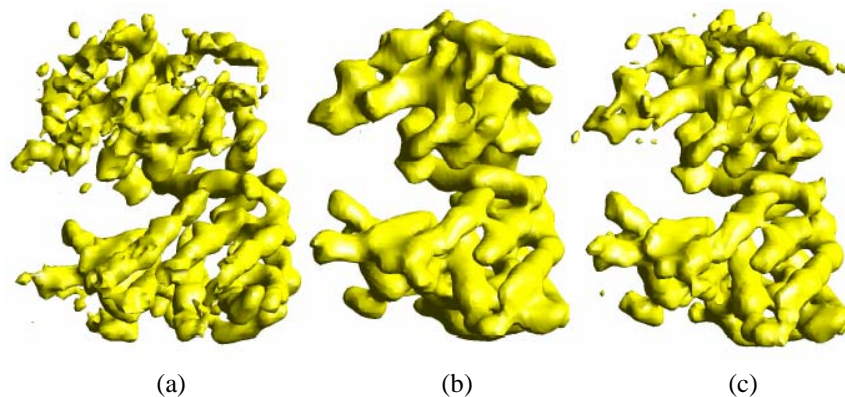


Figure 7. Comparative results between bilateral filtering and GDTV. (a), (b) and (c) show one subunit of (a), (b) and (c) of Figure 6.

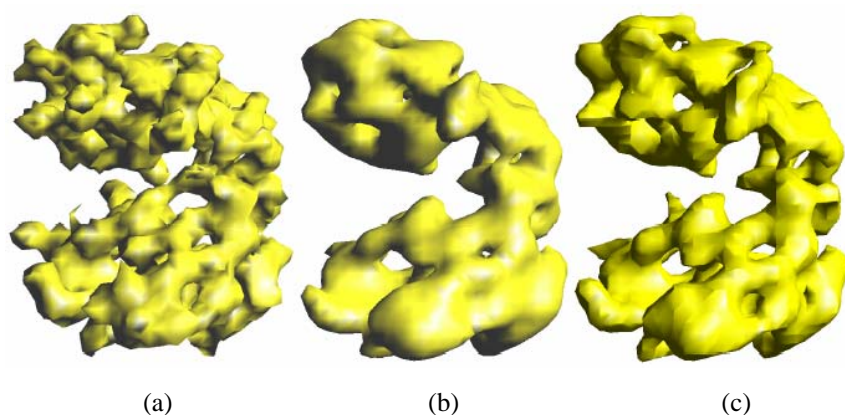


Figure 8. Comparative results between bilateral filtering and GDTV for 6Å GroEL density map. (a) shows one subunit segmented by the approach in [2, 30]. (b) shows the bilateral filtering result. (c) shows the result of GDTV.

5. Conclusion

A general formulation of image denoising method based on the variation of digitalized energy functional is presented. We generalize the generalized digitalized total variation method to 3D image. From the general energy functional, we derive the explicit iterative scheme. Large number of comparison experiments are carried out to verify the effectiveness of the proposed method. Our method is efficient, which is important because the 3D data quantity is always huge.

Acknowledgement

All the rendering and isosurface extraction approach are carried out in our image processing and visualization software tool VolRover. The figures are drawn with TexMol, another open source in-house software <http://cvcweb.ices.utexas.edu/software/#TexMol>. Figure 6 is produced by the software Chimera [24].

References

- [1] G. Aubert and P. Kornprobst, *Mathematical Problems in Image Processing, Partial Differential Equations and the Calculus of Variations*, 2nd ed., Applied Mathematical Sciences, Vol. 147, Springer, New York, 2006.
- [2] M. L. Baker, Z. Yu, W. Chiu and C. Bajaj, Automated segmentation of molecular subunits in electron cryomicroscopy density maps, *J. Struct. Bio.* 156 (2006), 432-441.
- [3] W. Baumeister, Electron tomography: Towards visualizing the molecular organization of the cytoplasm, *Curr. Opin. Struct. Biol.* 12 (2002), 679-684.
- [4] S. Bougleux, A. Elmoataz and M. Melkemi, Discrete regularization on weighted graphs for image and mesh filtering, *Scale Space and Variational Methods in Computer Vision*, F. Sgallari, A. Murli and N. Paragios, eds., Vol. 4485, Lecture Notes in Computer Science, 2007, pp. 128-139.
- [5] S. Bougleux, A. Elmoataz and M. Melkemi, Local and nonlocal discrete regularization on weighted graphs for image and mesh processing, *Internat. J. Comput. Vision*, 2008. <http://www.springerlink.com/content/5318217447616828/>
- [6] K. Braig, P. D. Adams and A. T. Brunger, Conformational variability in the refined structure of the chaperonin GroEL at 2.8Å resolution, *Nat. Struct. Biol.* 2 (1995), 1083-1094.
- [7] K. Braig, Z. Otwinowski, R. Hegde, D. C. Boisvert, A. Joachimiak, A. L. Horwich and P. B. Sigler, The crystal structure of the bacterial chaperonin GroEL at 2.8Å, *Nature* 371 (1994), 578-586.
- [8] T. F. Chan, S. Osher and J. H. Shen, The digital TV filter and nonlinear denoising, *IEEE Trans Image Processing* 10(2) (2001), 231-241.
- [9] T. F. Chan and J. H. Shen, *Image Processing and Analysis, Variational, PDE, Wavelet, and Stochastic Methods*, Society for Industrial and Applied Mathematics (SIAM), Philadelphia, 2005.
- [10] C. Chaudhry, A. L. Horwich, A. T. Brunger and P. D. Adams, Exploring the structural dynamics of the E. coli chaperonin GroEL using translation-libration-screw crystallographic refinement of intermediate states, *J. Mol. Biol.* 342 (2004), 229-245.

- [11] W. Chiu, What does electron cryomicroscopy provide that X-ray crystallography and NMR spectroscopy cannot?, *Ann. Rev. Biophys. Biomol. Struct.* 22 (1993), 233-255.
- [12] R. J. Ellis, der Vies S. M. van, Molecular chaperones, *Annu. Rev. Biochem.* 60 (1991), 321-347.
- [13] R. J. Ellis, Molecular chaperones, opening and closing the Anfinsen cage, *Curr. Biol.* 4(7) (1994), 633-635.
- [14] J. Frank, Single-particle imaging of macromolecules by cryo-electron microscopy, *Annu. Rev. Biophys. Biomol. Struct.* 31 (2002), 303-319.
- [15] R. M. Glaeser and K. A. Taylor, Radiation damage relative to transmission electron microscopy of biological specimens at low temperature: A review, *J. Microsc.* 112 (1978), 127-138.
- [16] R. C. Gonzalez and R. E. Woods, *Digital Image Processing*, 3rd ed., Prentice Hall, 2007.
- [17] L. S. Itzhaki, D. E. Otzen and A. R. Fersht, Nature and consequences of GroEL-protein interactions, *Biochemistry* 34 (1995), 14581-14587.
- [18] W. Jiang, M. L. Baker, Q. Wu, C. L. Bajaj and W. Chiu, Applications of a bilateral denoising filter in biological electron microscopy, *J. Struct. Bio.* 144 (2003), 114-122.
- [19] S. Kim and H. Lim, A non-convex diffusion model for simultaneous image denoising and edge enhancement, *Proceedings of the Sixth Mississippi State-UBA Conference on Differential Equations and Computational Simulations*, 175-192, *Electron. J. Differ. Equ. Conf.*, 15, Southwest Texas State Univ., San Marcos, TX, 2007.
- [20] S. J. Ludtke, M. L. Baker, D. Chen, J. Song, D. T. Chuang and W. Chiu, De novo backbone trace of GroEL from single particle electron cryomicroscopy, *Structure* 16 (2008), 441-448.
- [21] M. Lysaker, A. Lundervold and X. C. Tai, Noise removal using fourth-order partial differential equation with applications to magnetic resonance images in space and time, *IEEE Trans Image Processing* 12(12) (2003), 1579-1590.
- [22] J. Martin, T. Langer, R. Boteva, A. Schramel, A. L. Horwich and F. U. Hartl, Chaperonin-mediated protein folding at the surface of GroEL through a 'molten globule'-like intermediate, *Nature* 352 (1991), 36-42.
- [23] S. Osher and J. Shen, Digitized PDE method for data restoration, *Handbook of Analytic-computational Methods*, G. Anastassiou, ed., Applied Mathematics, Chapman & Hall/CRC, 2000, pp. 751-771.
- [24] E. F. Pettersen, T. D. Goddard, C. C. Huang, G. S. Couch, D. M. Greenblatt, E. C. Meng and T. E. Ferrin, UCSF chimera - a visualization system for exploratory research and analysis, *J. Comput. Chem.* 25(13) (2004), 1605-1612.

- [25] N. A. Ranson, D. K. Clare, G. W. Farr, D. Houldershaw, A. L. Horwich and H. R. Saibil, Allosteric signaling of ATP hydrolysis in GroEL-GroES complexes, *Nat. Struct. Mol. Biol.* 13 (2006), 147-152.
- [26] L. Rudin, S. Osher and E. Fatemi, Nonlinear total variation based noise removal algorithms, *Physica D* 60 (1992), 259-268.
- [27] L. Rudin and S. Osher, Total variation based image restoration with free local constraints, Vol. 1, *Proceedings of the IEEE International Conference on Image Processing*, 1994, pp. 31-35.
- [28] J. Sun, Q. Zhang, F. Wang and X. Zhao, On the generalization of digital total variation filter, Vol. 3, *Proceedings of First International Congress on Image and Signal Processing (CISP 2008)*, 2008, pp. 384-388.
- [29] Z. Xu, A. L. Horwich and P. B. Sigler, The crystal structure of the asymmetric GroELGroES-(ADP)₇ chaperonin complex, *Nature*. 388 (1997), 741-750.
- [30] Z. Yu and C. L. Bajaj, Computational approaches for automatic structural analysis of large biomolecular complexes, *IEEE/ACM Trans. Comput. Bio. Bioinf.* 5(4) (2008), 568-582.
- [31] Q. Zhang, J. Sun and G. Xu, Noise removal based on the variation of digitalized energy, *Proceedings of Geometric Modeling and Processing (GMP)*, F. Chen and B. Jüttler, eds., *Lecture Notes in Comput. Sci.*, Vol. 4975, Springer, Berlin, 2008, pp. 290-303.

Paper No. PPH-0910097-AM

Kindly return the proof after correction to:

*The Publication Manager
Pushpa Publishing House
Vijaya Niwas
198, Mumfordganj
Allahabad-211002 (India)*

along with the print charges*
by the fastest mail

***Invoice attached**

Proof read by:

Copyright transferred to the Pushpa
Publishing House

Signature:

Date:

Tel:

Fax:

e-mail:

Number of additional reprints required

.....
Cost of a set of 25 copies of additional
reprints @ U.S. Dollars 15.00 per page.

(25 copies of reprints are provided to the
corresponding author ex-gratis)